

Article

What Made the Sustained Intensification of Tropical Cyclone Fani in the Bay of Bengal? An Investigation Using Coupled Atmosphere–Ocean Model

Kumar Ravi Prakash¹, Vimlesh Pant^{1,*} , T. V. S. Udaya Bhaskar² and Navin Chandra¹ 

¹ Centre for Atmospheric Sciences, Indian Institute of Technology Delhi, New Delhi 110016, India; kravi1220@gmail.com (K.R.P.); navinchandra2003@gmail.com (N.C.)

² Indian National Centre for Ocean Information Services, Hyderabad 500090, India; uday@incois.gov.in

* Correspondence: vimlesh@cas.iitd.ac.in

Abstract: The extremely severe tropical cyclone Fani (25 April–5 May 2019) unusually sustained high intensity for a prolonged duration over the Bay of Bengal (BoB). A regional coupled atmosphere–ocean model was used to investigate the atmospheric and oceanic conditions and processes responsible for the sustained intensification of the tropical cyclone (TC) Fani. The coupled model simulated the track and intensification/weakening stages of the cyclone reasonably well. A reduction in sea surface temperature (by $-2\text{ }^{\circ}\text{C}$) and an increase in sea surface salinity due to cyclone-induced upwelling and inertial mixing was noticed in both observations and model. The passage of TC Fani over two geostrophic mesoscale warm-core eddies along the cyclone track was found to supply the necessary energy for the intensification of TC Fani. The sea surface height anomaly and tropical cyclone heat potential (TCHP) were higher during TC Fani than other pre-monsoon cyclones in the BoB. The anomalous TCHP in the warm-core eddy zones (i.e., in excess of $>160\text{ kJ cm}^{-2}$) maintained the warm surface temperature and high air–sea heat fluxes. The air–sea latent heat flux and atmospheric wind shear were favourable for the intensification of the cyclone. The atmospheric moist static energy enhanced up to 360 kJ kg^{-1} with a deep vertical extension in the atmospheric column supporting the further intensification of TC Fani. Therefore, the unusual oceanic TCHP associated with mesoscale eddies, higher latent heat flux, and enhanced moist static energy in the atmosphere contributed to the sustained intensification of TC Fani for a prolonged period in the BoB.

Keywords: tropical cyclone; Fani; Bay of Bengal; atmosphere–ocean model; latent heat flux; moist static energy



Citation: Prakash, K.R.; Pant, V.; Udaya Bhaskar, T.V.S.; Chandra, N. What Made the Sustained Intensification of Tropical Cyclone Fani in the Bay of Bengal? An Investigation Using Coupled Atmosphere–Ocean Model. *Atmosphere* **2022**, *13*, 535. <https://doi.org/10.3390/atmos13040535>

Academic Editors: Antonio Ricchi, Giovanni Liguori, Rossella Ferretti, Alvise Benetazzo and Francesco Barbariol

Received: 6 March 2022

Accepted: 25 March 2022

Published: 28 March 2022

Publisher's Note: MDPI stays neutral with regard to jurisdictional claims in published maps and institutional affiliations.



Copyright: © 2022 by the authors. Licensee MDPI, Basel, Switzerland. This article is an open access article distributed under the terms and conditions of the Creative Commons Attribution (CC BY) license (<https://creativecommons.org/licenses/by/4.0/>).

1. Introduction

Tropical cyclones (TCs) are one of the life-threatening weather phenomena. The strong wind generated from TCs produces storm surges and brings heavy rain, which causes inundation over coastal regions. The sea surface temperature (SST) is one of the most critical parameters for the genesis and intensification of the TCs process [1,2]. The ocean provides energy to TCs through surface heat fluxes. This energy is available in the upper few meters of the ocean and depends on the direction of local current and profiles of temperature and salinity. The upper-ocean temperatures help with TC development and maintenance. TCs associated with strong winds create instability in the upper ocean and generate divergent outward flows through local processes [3,4]. The TC-associated wind vector moves clockwise on the right of the TC track, which is generally resonant with the current in the mixed layer and displays higher cooling (lowering the sea surface temperature) on the right side of the cyclone track [3,5,6]. This cooling is due to the combined effects of heat loss by latent and sensible heat fluxes across the air–sea interface of the storm, a balance between the horizontal divergence of wind-driven currents, and turbulent vertical entrainment of colder thermocline waters across the oceanic mixed layer (OML). When sea surface cooling is

strong enough to balance or overcome the TC energy, the TC decays. Therefore, the sea surface cooling response to TC forcing is a crucial process for TC intensification.

A mesoscale eddy over the ocean plays an important role in deriving local circulation and dynamics. During the TC, the presence of these eddies can impact the oceanic response by changing the rate of upwelling and entrainment [7]. It has been suggested that pre-existing positive sea surface height anomaly (SSHA) features or anticyclonic ocean eddies (ACOE) play essential roles in the upper ocean's response to cyclones. Several studies suggested rapid TC intensification when the storms interact with warm ocean eddies [8–11]. The mesoscale eddies are a prominent feature of the BoB. The highest eddy kinetic energy (EKE) activated regions of BoB are identified and studied by [12]. The east of Sri Lanka, northwest of Sumatra, the western BoB and the coastal rim of BoB are the EKE dominating areas, and each area produces a high magnitude of EKE by virtue of different oceanic processes and their combinations [12]. The seasonal presence of these eddies is seen in the regions as mentioned above [13]. The mesoscale eddies can be treated as baroclinic instabilities. The TCs over BoB are predominant in the April–June and October–December months. During these two different time spans of favourable season for TCs, two different eddy features (cyclonic and anticyclonic) were also confined over a large area of north BoB.

The low-pressure systems and tropical cyclones formed over the north Indian Ocean are classified based on the associated wind speed by the India Meteorological Department (IMD). A deep depression (DD; 50–61 km/h) can intensify into a cyclonic storm (CS; 62–87 km/h). The system is termed a severe cyclonic storm (SCS) when winds range from 88 to 117 km/h. A further intensification of the system makes it a very severe cyclonic storm (VSCS; 118–167 km/h). The extremely severe cyclonic storm (ESCS) has a wind speed of the order of 168–221 km/h. Any further increase in the wind speed (>222 km/h) takes it to the super cyclone (SuCS) category. The higher category (i.e., stronger wind speed) of cyclone is associated with larger disasters in coastal regions in terms of storm surge, coastal inundation (or flooding), torrential precipitation and impacts on coastal infrastructure, livelihood, and marine ecosystem.

Fani cyclone was an extremely severe cyclonic storm. It was the most intense cyclonic storm during pre-monsoon season that ever crossed over Odisha state in eastern India. It was originated at 2.70° N and 88.70° E in the morning at 05:30 GMT of 25 April 2019. It moved nearly northwestwards, converted into a DD and further into a CS category by 11:30 GMT on 27 April over the southeastern BoB. After that, it moved northwestwards and transformed into an SCS category. TC Fani relocated northwards while it was intensified into a VSCS. It moved west-northwestwards and further intensified into an extremely severe cyclonic storm (ESCS) on 30 April at 17:30 GMT. It started changing the path toward north-northeastwards and continuously intensified until 14:30 GMT on 2 May, reaching the peak intensity of 213 km/h. It crossed the Odisha coast close to Puri as an ESCS with a maximum sustained wind speed of 204 km/h from 08:00 to 10:00 GMT on 3 May 2019. It was a unique tropical cyclone that remained continuously intensified for a long duration in the shallow depth and made landfall in the ESCS category. The mean duration of all TCs in the ESCS category over the BoB is 22 h whereas, for the TC Fani it was more than 60 h duration in the ESCS category. TC Fani spent more time in the ESCS category as compared to any other cyclones over the BoB (Figure 1).

Based on the unique characteristics of TC Fani, the present study is focused on identifying the causative mechanisms or processes promoting the sustained intensification of Fani cyclone for a long time in the ESSC category over the shallow coastal region.

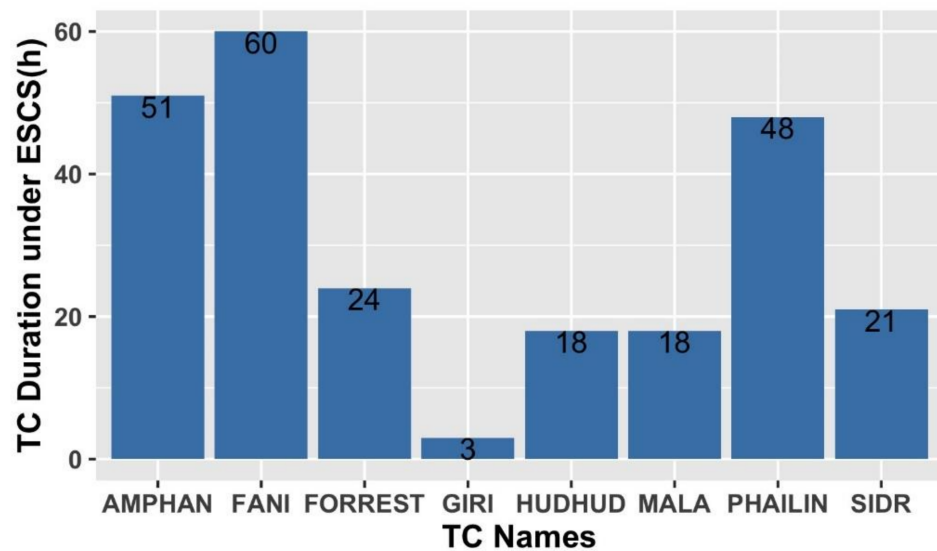


Figure 1. Duration (in hours) of tropical cyclones in the extremely severe cyclonic storm (ESCS) category over the BoB. TC names are mentioned along with the number of hours spent in the ESCS category on each bar. Data used for the duration of years 1990–2020 from the IMD data available from IBTrACS (<https://www.ncei.noaa.gov/data/international-best-track-archive-for-climate-stewardship-ibtracs/v04r00/access/csv/>) (accessed on 15 December 2021).

2. Data and Methodology

Model Details and Configuration

The coupled ocean–atmosphere–wave–sediment transport (COAWST) modelling system [14] was utilized for this study. In the present study, the coupled atmosphere–ocean version of the COAWST modelling system was used without the wave model. The COAWST model has been used widely for the simulation of cyclones/hurricanes and associated processes [15–18].

The atmospheric model Weather Research and Forecasting (WRF) [19] is used in the coupled model systems. It is configured as a fully compressible and non-hydrostatic model with various physical parameterization schemes. The model is used with two nested domains (shown in Figure 2) with a resolution of 9 km and 3 km in the outer and inner domains, respectively. The inner domain is movable that follows the TC vortex. Time steps for WRF domains were 30 s and 10 s for the outer and inner domains, respectively. Except for the planetary boundary layer and the closure scheme, all other parameterizations used in this study are the same as in [18]. In this study, the Mellor–Yamada Nakanishi Niino (MYNN) level 2.5 [20–23] closure scheme for the planetary boundary layer is used. The atmospheric model WRF was initialized on 29 April 2019 at 00 GMT using initial and boundary conditions from the National Centre for Environmental Prediction (NCEP) Final Analysis (FNL) data with a resolution of $1^\circ \times 1^\circ$ [24]. The lateral boundary conditions were updated at 6 h intervals.

The ‘Regional Ocean Modeling System’ (ROMS) is utilized as an ocean model in the COAWST system. It is a free surface terrain-following three-dimensional numerical model which solves Reynolds–Averaged Navier–Stokes (RANS) equations using the hydrostatic and Boussinesq assumptions [25,26]. For this study, the horizontal resolution of the ROMS model was $1/24^\circ \times 1/24^\circ$ and a total of 40 vertical sigma levels were used. The remaining parameterization scheme and constant parameters used in the study was the same as in [18]. We provided TPXO7.2 derived all the 13 tidal constituents at the open boundaries. The vertical stretching parameters in the ROMS model are set at $\theta_s = 7$, $\theta_b = 2$. The critical depth (Tcline) is kept as 1 m. The model time steps for baroclinic (slow) and barotropic (fast) simulation were fixed at 20 s and 30 s, respectively. The K- ϵ turbulence closure model is used for the sub-grid scale vertical mixing. The Generic Length-Scale (GLS)

as described by [27] was adopted in the COAWST modelling system by [28]. A model coupling toolkit (MCT) was used to exchange variables among the components of the COAWST modelling system [29,30]. The exchange of the prognostic variables within the model components were made at every 600 s. Further detail of the COAWST modelling system can be found in [14]. The WRF model exchanges variables atmospheric surface pressure, zonal and meridional surface wind, relative humidity, surface air temperature, shortwave and longwave radiation, and cloud and rain rate with the ocean model ROMS at every 10 min interval. At the same time, the ROMS model passes SST information to the WRF model, which helps to improve air–sea heat fluxes in the model. Further details of the exchange of variables in the WRF–ROMS coupled model are provided in [31].

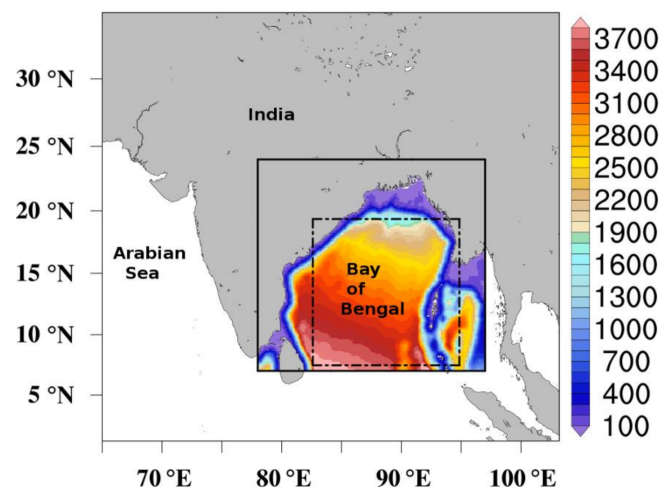


Figure 2. Model domains of atmospheric (WRF) and ocean (ROMS) models. The outermost boundary shows the outer domain of the WRF model. The inner movable domain of the WRF model is shown with a dashed line. The ROMS model domain is shown with a continuous line with shades representing ocean bathymetry (m).

The coupled atmosphere–ocean (WRF–ROMS) model was configured over the BoB domain of 78° E–97° E and 7° N–24° N as shown in Figure 2. The area bounded by a square drawn in a dashed line shows the boundary of the inner movable domain of the WRF model, which follows the centre of the tropical cyclone as it propagates over the BoB. The outermost border of the domain represents the outer domain of the WRF model. The re-positioning of the inner domain occurs at 30 min intervals enabling maintaining a centre for the cyclone (i.e., the minimum pressure) inside the high-resolution inner domain. The ROMS model domain is shown with a solid continuous line covering the BoB region. The coupling between ROMS and WRF models was conducted in such a way that both the WRF model domains interact with the ROMS model. Numerical simulations are performed from 29 April (00:00 GMT) to 4 May (00:00 GMT) 2019. The initial and lateral open boundary conditions in the ROMS model were derived from the HYCOM data (from 29 April to 4 May 2019 at daily time intervals and 1/12 degree resolution) and bathymetry was derived from the Gridded Global Relief Data (ETOPO2) with 2 min resolution.

3. Results and Discussion

3.1. Track and Intensity Simulation of TC Fani

Figure 3 shows the coupled-model-simulated track (red curve) together with the best-track (black curve) of TC Fani reported by IMD. The 3-hourly positions of the cyclone's centre are marked with dots on both tracks. Additionally drawn in the figure is the cone of uncertainty provided by IMD using ensemble model runs at different hours during the progress of TC Fani. It can be inferred from the figure that the model-simulated track is well within the projected cone of uncertainty by IMD. However, there is a mean error of the order of 100 km in the simulated track with respect to the IMD best-track. IMD

provides the best-track estimate of a cyclonic storm based on various observations and models [32]. A validation of simulated wind speed and mean sea level pressure (MSLP) at the locations of buoys BD11 and BD13 (marked with blue circles in Figure 3) is shown in Figure 4. There was no spatial or temporal interpolation performed on the buoy or model data. The simulated values are considered from the model grid where the buoy was located. It is worth noting that BD11 was in close proximity to Fani's track whereas BD13 was at a distance of about 250–300 km from the TC track. The temporal variations in surface wind speed and MSLP are captured well by the model at the BD11 location. However, there was a data gap in BD11 measurements during the high-intensity period of TC Fani after 15 GMT on 30 April. The continuous measurements at BD13 mark the typical features of cyclone's passage as an increase in wind speed and drop in MSLP as the cyclone approaches this location. With the departure of the cyclone over this location, wind speed and MSLP gradually restored to the pre-cyclone values. At the BD13 location, the coupled model simulates the intensification and weakening stages of TC Fani in accordance with the buoy measurements for the simulation period. For wind speed, the RMSE was 2.9 (3.6) m/s for BD11 (BD13) and correlation was 0.92 (0.64) at BD11 (BD13) locations. For MSLP, the RMSE was 4.13 (1.62) hPa for BD11 (BD13) and correlation was 0.94 (0.89) at BD11 (BD13) locations. Compared to an uncoupled model, the fully coupled COAWST model was found to have a modest improvement in track and significant improvement in intensity simulation of hurricane Ivan [15]. The sea surface temperature (SST) recorded at a drifting buoy (marked by a green star in Figure 3) is plotted in Figure 5. The model-simulated SST time series at this location is also plotted for the duration of the simulation. It is clear from the figure that the ocean model ROMS in the coupled model represents the SST variations realistically. The decrease in SST from the middle of 30 April can be seen in both model and observation. This surface cooling is associated with the TC Fani by means of cyclone-induced upwelling and inertial mixing [33,34].

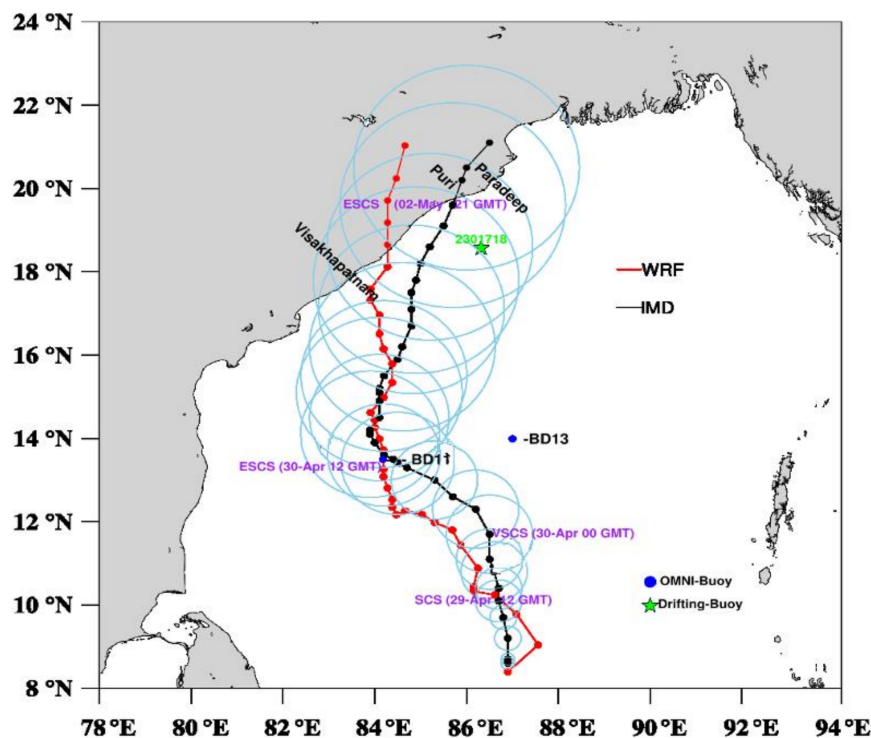


Figure 3. Model computed Fani cyclone track (00 GMT on 29 April to 00 GMT 3 May) along with IMD best-track. Locations of buoys are marked with different symbols and colours. The light blue circle represents the cone of uncertainty at different hours from IMD data.

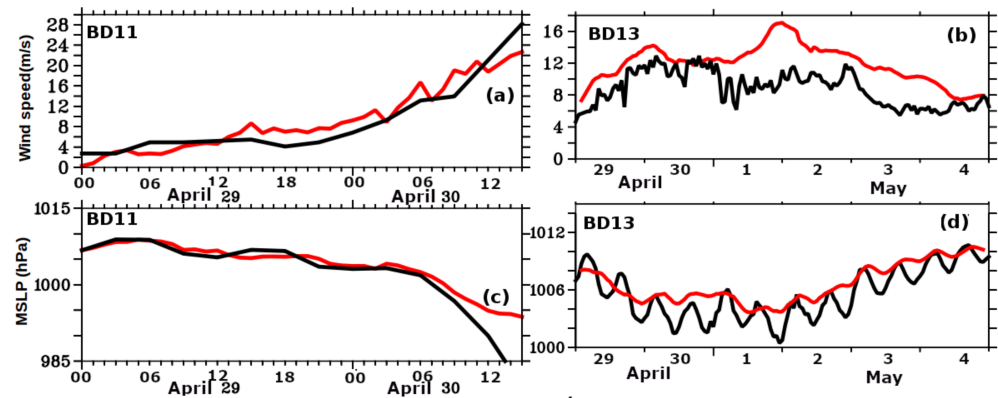


Figure 4. Comparison of model simulation (red) and observed (black) wind speed (a,b) (m/s) and mean sea level pressure (c,d) (hPa) at buoys BD11 and BD13 (buoy locations marked in Figure 3).

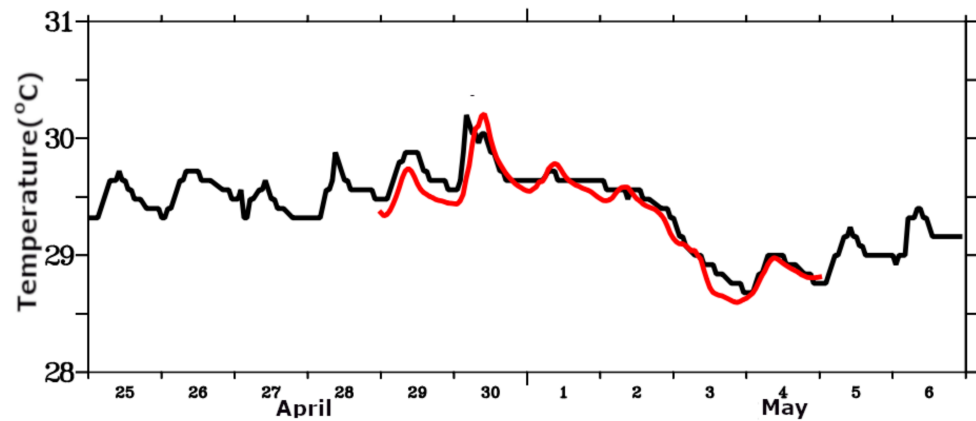


Figure 5. Comparison of sea surface temperature (°C) simulated by model (red) against drifting buoy measured (black). The location of the drifting buoy is marked in Figure 3.

The spatial patterns of SST, surface circulation, and salinity as simulated by the coupled model are presented in Figure 6. These parameters are plotted at 00 GMT each day from 29 April to 4 May 2019. Variation in the daily SST pattern is validated against GHRST (Group for High-Resolution Sea Surface Temperature) data (accessed on 10 February 2020 from <https://doi.org/10.5067/GHGMR-4FJ04>). The GHRST data have a resolution of 0.05° [35]. However, the daily surface currents and surface salinity could not be validated due to the non-availability of these data on a daily time scale. Surface currents plotted for each day clearly show the cyclonic circulation appearing in the southern BoB on 29 April with a magnitude of up to 1.8 ms^{-1} . This cyclonic current pattern moves northwestward towards the Indian coastline on 30 April–1 May. Surface currents then follow the track of TC Fani and are seen interacting with the East India Coastal Current.

From 29 April to 1 May, the SST pattern shows colder sea surface in the southern BoB than in the northern bay by virtue of lower net heat flux over the cyclone influenced region in the south. On 2 May, a patch of pronounced surface cooling (by 2°C) was visible in the east-central bay (centred around 13°N , 85°E) in both observation and model. However, the cooling is marginally higher in the model and confined to a smaller region than observations. This significant cooling of SST is primarily due to the cyclone-induced upwelling resulting from the offshore Ekman mass transport at the surface by the cyclonic wind stress. Further, the shear generated under the storm conditions penetrates to the thermocline depth leading to aggressive mixing of colder water in the mixed layer by near-inertial oscillations [31]. The model captured another patch of surface cooling near the Indian coast on 4 May when the TC Fani passed over this region. The SST bias is generally observed in ocean models. The coupled atmosphere–ocean models were found to have less

SST bias than the uncoupled ocean model [14,31,36]. In the current study, an SST bias of up to 2 °C is noticed against satellite-derived SST which could be associated with the errors in model parameterization schemes, initial and boundary conditions, representation of small scale processes, and errors in satellite-derived SST data used for validation. However, this SST bias does not affect the overall finding presented in the paper as most of the analysis is based on the TCHP which is the integrated heat from the surface up to the 26 degree isotherm depth. A better comparison of model-simulated SST is seen with in-situ measured SST (shown in Figure 5). Associated with cyclone-upwelling, there is a signature of enhanced surface salinity after 2 May in model simulations. The magnitude of increase in the sea surface salinity is up to 1.2 psu. The BoB is known for its well-stratified thermohaline structure due to the surplus amount of freshwater in the upper few tens of meters which maintain a strong haline stratification [37–40]. The high salinity water below 30 m depth gets pulled up into the mixed layer under the upwelling process.

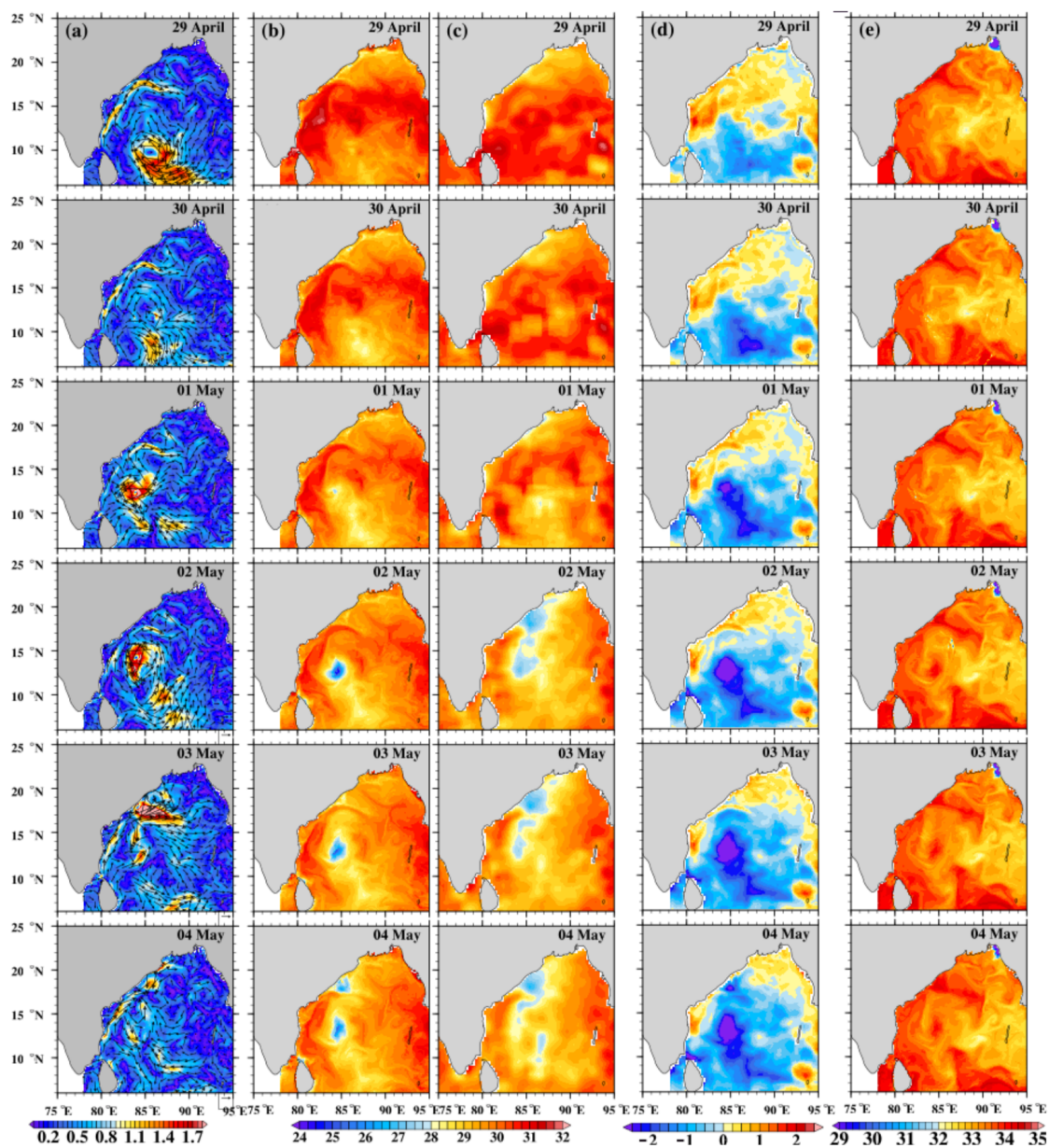


Figure 6. At 00 GMT each day: (a) model-computed surface current (m/s), (b) model-computed sea surface temperature (°C), (c) observed sea surface temperature from GHRSSST, (d) difference (model–observation) in sea surface temperature, and (e) model-computed sea surface salinity (psu).

3.2. Role of Oceanic Mesoscale Eddies

In order to understand the reasons for the sustained intensification of TC Fani, the background conditions of the ocean are analysed. It is found that the track of TC Fani traversed over a couple of oceanic mesoscale eddies. Ocean eddies have a cold (warm) core depending on their cyclonic (anticyclonic) nature. The presence of these eddies would certainly affect the fluxes of heat at the air–sea interface and, thereby, influence the cyclone’s intensity/track. The use of a fully coupled atmosphere–ocean model in the present study facilitates examining this aspect of air–sea heat and moisture fluxes over the eddy regions and their effects on the TC Fani.

A climatology of sea surface height anomaly (SSHA) and its standard deviation for April derived from ‘Archiving, Validation and Interpretation of Satellite Oceanographic data’ (AVISO) data are plotted in Figure 7. The figure also shows SSHA plotted for 29 April 2019 (the initial stage of the TC Fani) in the lower panel overlaid with the surface current vectors acquired from OSCAR (Ocean Surface Current Analysis Real-time) data at a resolution of one-third degree [41]. For reference, the IMD best-track of TC Fani with its intensity in colour codes is also drawn in the figure. The figure shows that the presence of mesoscale eddies of cyclonic and anticyclonic nature is a climatological feature during this time of the year. The time of the entry and exit of TC Fani in any of these eddies are marked with solid black circles in the lower panel of Figure 7. It can be seen from the figure that TC Fani first enters into the warm-core eddy (positive SSHA) at 21 GMT on 29 April and then briefly crosses over the cold-core eddy (negative SSHA) during 02–12 GMT on 30 April. TC entered the regime of a large warm-core eddy and remained over it until 03 GMT on 1 May and then progressed further in the northeastern direction along the Indian coastline. It is worth mentioning that TC Fani unusually remained intensified into the ESCS category from 12 GMT on 30 April to 21 GMT on 2 May (Figures 3 and 7). The TC became intensified from VSCS to ESCS category upon entering into the large warm-core eddy zone. However, it remained in the ESCS category for another 48 h after its exit from the warm-core eddy. Overall, the TC Fani remained in the ESCS category for more than 60 h. An intercomparison of SSHA values for 29 April 2019 (lower panel in Figure 7) with the April month’s climatology of SSHA highlights that the strength of the warm-core eddy in April 2019 was almost double that of the climatological eddy expected during this time of the year. The anomalous warm-core eddies interact with the cyclone through air–sea heat fluxes. The enhanced strength of eddies (i.e., higher SSHA) indicates high heat potential associated with these anticyclonic eddies which could help in the development of TC Fani. The impact of anomalous positive SSHA and other atmospheric and oceanic variables/conditions on the TC Fani characteristics are explored in the next section.

3.3. Impact of Anomalous Atmospheric and Oceanic Conditions

Several studies reported that the tropical cyclone heat potential (TCHP) is a crucial factor in determining the strength of TCs [42]. The TCHP is calculated as the heat stored in the upper ocean from the surface to the depth of the 26 °C isotherm. The following equation was used to calculate TCHP.

$$TCHP = \rho C_p \int_0^{D26} (T - 26) dz \quad (1)$$

where ρ is density and C_p is the specific heat of seawater. T is temperature and $D26$ is the depth of the 26 °C isotherm.

As TCHP measures the integrated vertical temperature of the ocean from the surface to the depth of the 26 °C isotherm ($D26$), it is, therefore, a measure of the heat energy of the ocean, it plays a significant role in the formation and intensification of tropical cyclones [4,8–11,43]. The ECCO2 (Estimating the Circulation & Climate of the Ocean) reanalysis data [44] with a resolution of 0.25° are used to calculate the TCHP over the BoB. Figure 8 shows climatological values of TCHP for 25 April–10 May (panel a) and standard

deviation of TCHP for April (panel b) during the period of years 2008–2018. In panel (c) of this figure, TCHP is plotted for 25–28 April 2019 (period of TC Fani). It can be noted from the figure that anomalously high TCHP was present during the occurrence of TC Fani in the BoB. While the climatological TCHP in the western BoB was up to 110 kJ cm^{-2} , its value was $>160 \text{ kJ cm}^{-2}$ during the period of TC Fani in April 2019, which was much above one standard deviation of TCHP. This excess heat content of the upper ocean helped fuel the cyclone to greater intensity. The region of higher TCHP in the bay was primarily associated with the mesoscale warm-core eddies.

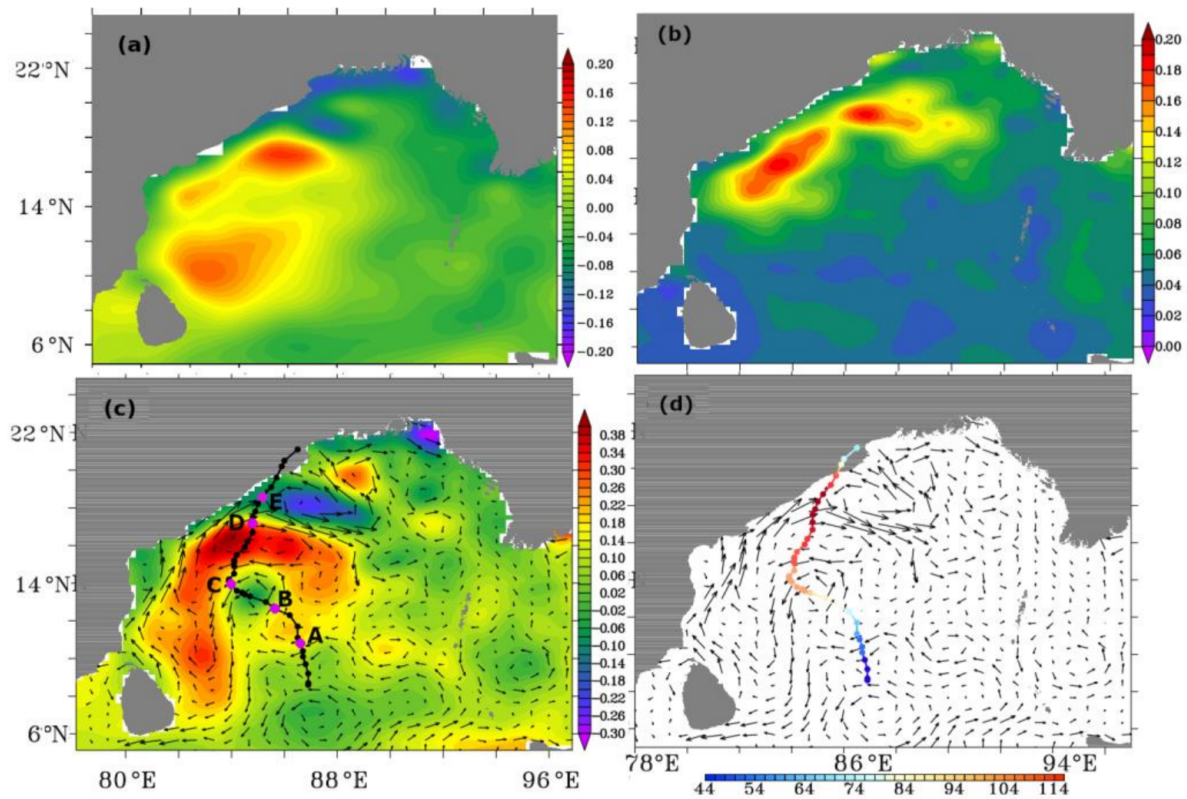


Figure 7. (a) Sea level anomaly (m) from AVISO climatology, (b) standard deviation of sea level anomaly (m) for April calculated from AVISO data, (c) sea level anomaly on 29 April 2019 overlay with OSCAR current vectors and IMD best-track of TC Fani, (d) OSCAR current vectors and IMD best-track with intensity (m/s) shown in colour shades. The black dots marked with A, B, C, D, E in panel (c) highlight the locations where the TC enters into or exits from a cyclonic or anticyclonic eddy.

The heat is supplied to the atmosphere by means of sensible and latent heat fluxes over the high TCHP regions, which are conducive for the intensification of a cyclone. As a consequence of higher evaporation and latent heat flux over the anticyclonic eddy zone, the moisture content in the atmospheric column increases. This leads to the enhancement of moist static energy (MSE) in the atmosphere, promoting convection and, hence, cyclone intensification via conversion of potential energy to kinetic energy. Figure 9 shows the coupled-model-simulated MSE in the atmospheric column over the selected locations (marked with dots A to E in Figure 7) along the track of TC Fani. An enhancement in MSE can be seen in the figure when the cyclone enters into the warm-core (anticyclonic) eddy zone. At point 'A', the MSE was of the order of 350 kJ kg^{-1} that extended vertically up to $\sim 550 \text{ hPa}$ in the atmosphere. There was a rapid increase in the MSE as the cyclone moved further from point 'B' to 'C'. At the 'C' location, the cyclone entered into the larger anticyclonic eddy with higher TCHP (see Figure 7). As a result, the MSE increased to 356 kJ kg^{-1} on 1 May and further up to 360 kJ kg^{-1} on 2 May. The vertical extent of the MSE also reached up to 300 hPa level which provided the ancillary strength to the

cyclone. The TC Fani remained intensified for a long duration (about two days) during 1–3 May 2019. The passage of the Fani cyclone over the large warm-core eddies facilitated its sustained intensification.

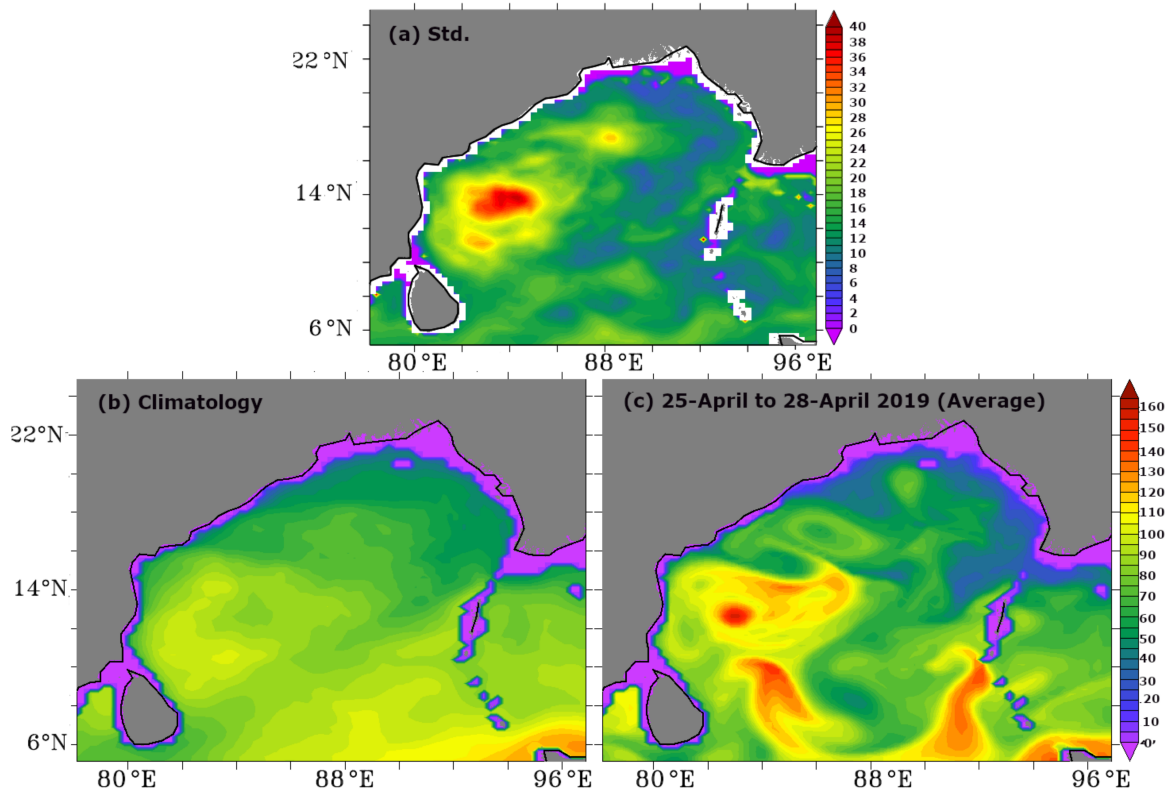


Figure 8. (a) Standard deviation of tropical cyclone heat potential (TCHP in kJ cm^{-2}) during April for the period of 2008–2018, (b) climatological TCHP (kJ cm^{-2}) calculated for the 2008–2018 period for 25 April–10 May, (c) TCHP during the passage of Fani cyclone over the BoB (25–28 April 2019).

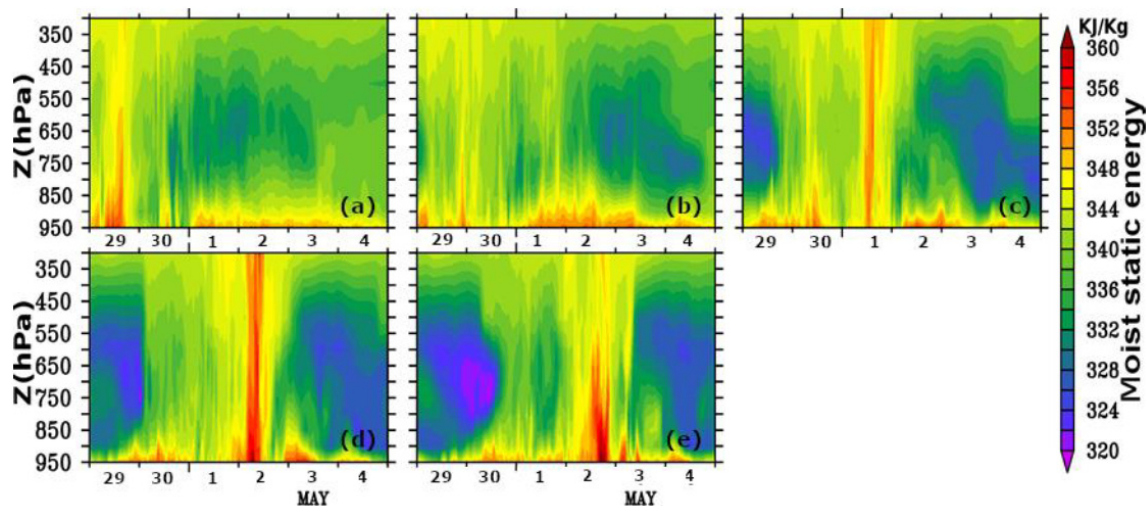


Figure 9. Model-simulated moist static energy (kJ kg^{-1}) over the locations A, B, C, D, E (marked in Figure 6) in panels (a–e), respectively.

The vertical wind shear in the atmosphere is an important detrimental factor for the cyclone’s intensification [7,45]. The coupled model-simulated vertical wind shear between the 850 hPa and 300 hPa levels is plotted in Figure 10 for each day at 00 GMT during the TC Fani. The pre-existing wind shear gradient was as low as 0.01 Nm^{-2} on 29 April.

The low wind shear conditions were found in advance over the region of TC movement. This low wind shear was maintained until 4 May, which supported the deep convection and sustained intensification of TC Fani. Figure 11 shows the model-simulated daily (at 00 GMT) latent heat flux over the BoB. The high values of latent heat flux ($>1000 \text{ W m}^{-2}$) can be noticed in the vicinity of the cyclonic vortex. High latent heat flux resulted from the passage of TC Fani over the large warm-core eddies with high TCHP (see Figures 7 and 8). A high TCHP ensures heat supply to the sea surface, where active heat flux exchange occurs between the atmosphere and the ocean. The warm-core eddies helped to maintain the TCHP under the strong wind-driven heat loss from the sea surface.

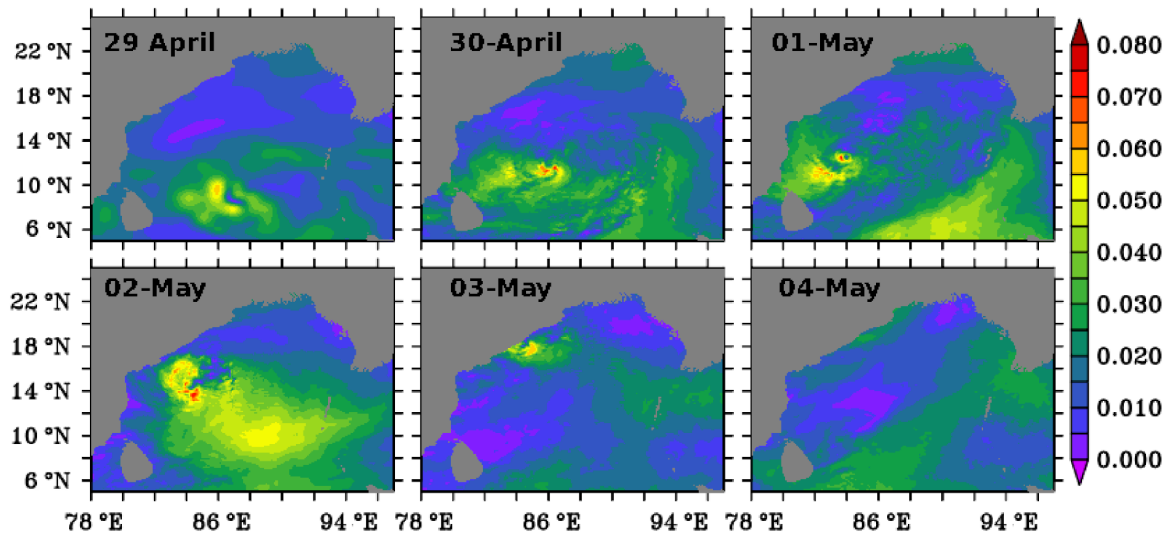


Figure 10. Model-simulated daily wind shear gradient (Nm^{-2}) (850–300 hPa) at 00 GMT each day for 29 April to 4 May 2019, during the passage of TC Fani over the BoB.

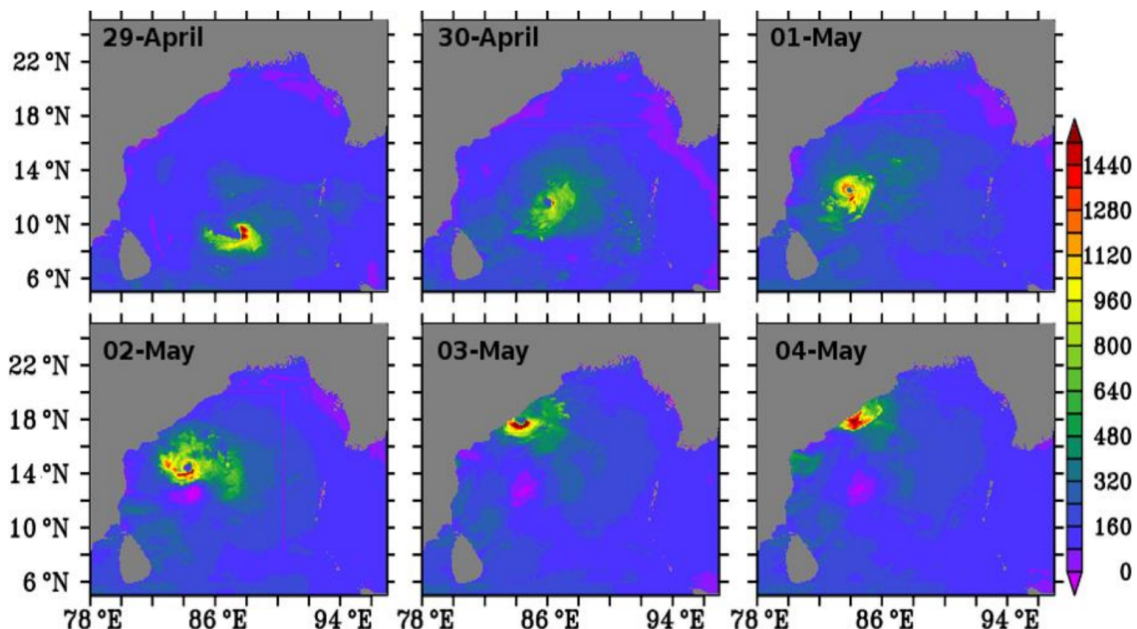


Figure 11. Model-simulated daily latent heat flux (Wm^{-2}) at 00 GMT each day for 29 April to 4 May 2019, during the passage of TC Fani over the BoB.

To understand the maintenance of high TCHP for a long duration, the time series of temperature profiles and stratification at points A, B, C, D, E (marked in Figure 7) are plotted in Figure 12. The near-surface temperature increased by 2–3 °C as the TC moved

from location A to B. The depth of warmer water also increased gradually under mixing in the eddy zone. A remarkable transition phase can be noticed in the temperature profiles from locations C to E during May 1–3. A signature of cyclone-induced upwelling and subsequent mixing can be seen on 2 May at location D and 3 May at location E. However, the deep (>120 m) extent of warm waters (>26 °C) associated with warm-core eddies before the arrival of TC Fani over locations D and E (i.e., before 1 May) ensured that SST remained warm enough (>28 °C) to sustain the intensity of TC Fani in the ESCS category. It explains the maintenance of high TCHP and latent heat flux during this period of sustained intensification of TC Fani as noted in Figures 8 and 11. A recent study highlighted the roles of Madden Julian Oscillation, warm surface and subsurface temperature in TC Fani intensification [46]. Another study [47] reported an interaction between the TCs and western boundary current in the BoB during Fani and Amphan cyclones. The warm SST and high evaporation increase latent heat flux leading to intensification of TCs [18,48]. Numerical sensitivity experiments indicated warmer SSTs supporting more energetic TCs and enhancing the chances of depressions growing into sizable TCs [49].

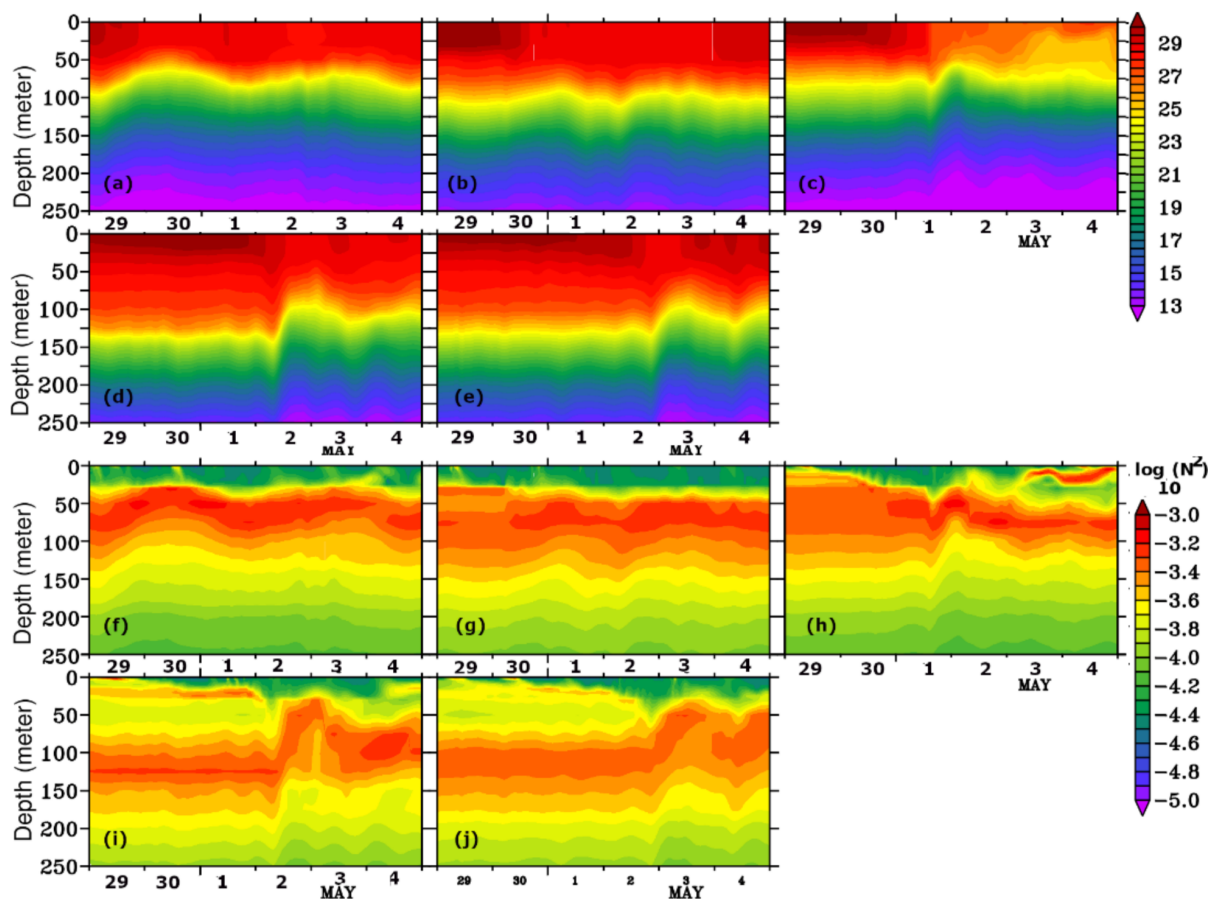


Figure 12. Time series of model-simulated profiles of temperature (°C) at locations A, B, C, D, E (marked in Figure 7) shown in panels (a–e), respectively. Stratification (i.e., buoyancy frequency) computed from model data at points A, B, C, D, E shown in panels (f–j), respectively.

The stratification represented by the buoyancy frequency (N) is calculated using Equation (2).

$$N^2 = -\frac{g}{\rho} \frac{\partial \rho}{\partial z} \tag{2}$$

where g is the acceleration due to gravity, z is depth, and ρ is the density of seawater. The magnitude of initial stratification at point A (panel f) reduced with time as the TC moved over locations B and C. The strong turbulent mixing under the cyclone weakened

the stratification and distributed heat in the water column. However, the stratified layer moved upward towards the surface on 1 May at location C (panel h). At locations D and E, the subsurface mixing continued and the position of stratification maxima remained around 50 m depth at locations D (panel i) and E (panel j), which restricted the entrainment of colder waters from below the thermocline.

For comparison, the along-track SSHA and TCHP are plotted for three TCs that crossed over the BoB and intensified into the ESCS category during the pre-monsoon season. TCs Mala (25–29 April 2006) and Amphan (16–21 May 2020) had lower positive SSHA than TC Fani, which signifies the presence of an anomalously strong warm-core eddy in the case of TC Fani. As a result of the anomalous eddy, the TCHP was much higher during TC Fani than TCs Mala and Amphan. Moreover, the high TCHP was maintained for a long duration during the passage of TC Fani (Figure 13). Therefore, the presence of anomalously strong anticyclonic (warm-core) eddies (Figure 7) supplied the necessary heat to maintain high TCHP and warm SST leading to a large latent heat flux and surplus moist static energy in the atmospheric column which resulted in the prolonged intensification of TC Fani in the ESCS category.

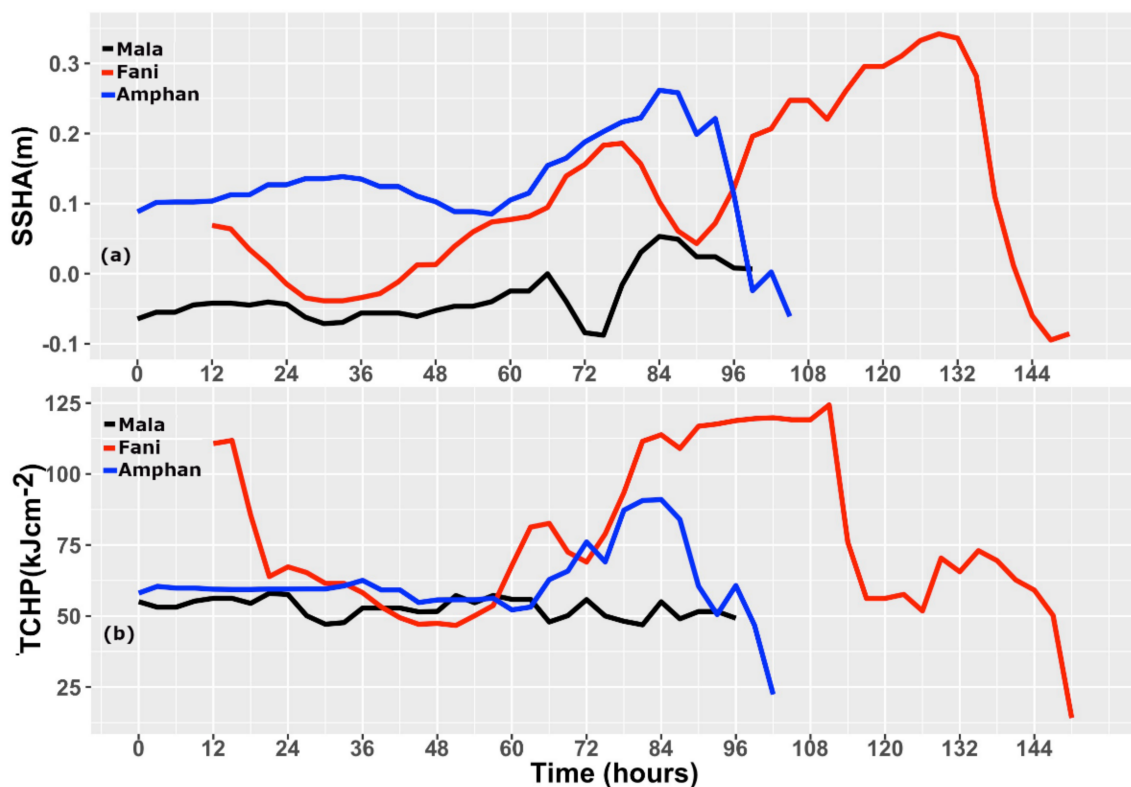


Figure 13. Along-track sea surface height anomaly (SSHA in m) (a) and along-track tropical cyclone heat potential (TCHP in kJ cm^{-2}) (b) for cyclones Mala, Fani, and Amphan formed over the BoB during the pre-monsoon season (April–May).

4. Conclusions

A coupled atmosphere–ocean model was used to simulate the tropical cyclone Fani which originated in and crossed over the BoB during 25 April–5 May 2019. The uniqueness of TC Fani was its prolonged sustenance in the extremely severe cyclonic storm category. The presence of two warm-core (anticyclonic) eddies en route the track of TC Fani was found to play a centric role in supporting the sustained intensification of the cyclone. The satellite-derived SSHA and upper ocean characteristics reveal that the eddy was almost double the strength, in April–May 2019, of the climatological warm-core eddy over this region. Further, the SSHA and TCHP along the track of Fani were higher than other ESCS category cyclones in the pre-monsoon season over the BoB. The anomalously high TCHP ($>160 \text{ kJ cm}^{-2}$)

associated with the strong mesoscale warm-core eddy ensured the continuous supply of necessary heat up to the sea surface and supported TC Fani intensification. The large heat content supported high latent heat flux at the air–sea interface and promoted convection leading to enhanced MSE in the atmospheric column. The MSE was found to rapidly increase to 360 kJ kg^{-1} with a vertical extent up to 300 hPa during 1–2 May 2019. The high MSE led to higher latent heat release in the atmosphere, which fuelled the TC Fani to greater intensity. Within the ocean, the cyclone-induced upwelling and mixing reduced the SST and weakened the stratification in the water column. However, the presence of anomalous anticyclonic eddies maintained the SST warm enough ($>28 \text{ }^\circ\text{C}$) to support TC Fani intensification during the upwelling and associated cooling period on 2–3 May. Therefore, the high latent heat flux and atmospheric MSE over the anomalously strong warm-core eddy ensured sustained intensification of TC Fani over the BoB.

Author Contributions: Data curation, T.V.S.U.B.; Formal analysis, K.R.P.; Investigation, K.R.P., V.P. and T.V.S.U.B.; Resources, V.P.; Software, K.R.P. and N.C.; Supervision, V.P.; Validation, N.C.; Visualization, N.C.; Writing—original draft, V.P.; Writing—review & editing, T.V.S.U.B. All authors have read and agreed to the published version of the manuscript.

Funding: This research received no external funding. The APC was funded by IIT Delhi.

Institutional Review Board Statement: Not applicable.

Informed Consent Statement: Not applicable.

Data Availability Statement: Links to the data sources used in this study are provided in the manuscript. Our model data is available on request from the corresponding author.

Acknowledgments: Authors acknowledge the National Institute of Ocean Technology, Chennai and Indian National Centre for Ocean Information Services, Hyderabad for providing OMNI buoy (BD11 and BD13) data (accessed on 20 October 2020 from <http://www.incois.gov.in/portal/index.jsp>, 17 October 2021). ECCO2 is a contribution to NASA modelling analysis and MAP program. The high-performance computing (HPC) facility provided by IIT Delhi and the Department of Science and Technology (DST-FIST 2014 at CAS), Government of India, are thankfully acknowledged.

Conflicts of Interest: The authors declare no conflict of interest.

References

1. Bender, M.A.; Ginis, I.; Kurihara, Y. Numerical simulations of tropical cyclone-ocean interaction with a high-resolution coupled model. *J. Geophys. Res. Atmos.* **1993**, *98*, 23245–23263. [[CrossRef](#)]
2. Mahapatra, D.K.; Rao, A.D.; Babu, S.V.; Srinivas, C. Influence of coast line on upper ocean's response to the tropical cyclone. *Geophys. Res. Lett.* **2007**, *34*, L17603. [[CrossRef](#)]
3. Price, J.F. Upper ocean response to a hurricane. *J. Phys. Oceanogr.* **1981**, *11*, 153–175. [[CrossRef](#)]
4. Lin, I.-I.; Liu, W.T.; Wu, C.-C.; Wong, G.T.F.; Hu, C.; Chen, Z.; Liang, W.-D.; Yang, Y.; Liu, K.-K. New evidence for enhanced ocean primary production triggered by tropical cyclone. *Geophys. Res. Lett.* **2003**, *30*, 1718. [[CrossRef](#)]
5. Dickey, T.D.; Simpson, J.J. The influence of optical water type on the diurnal response of the upper ocean. *Tellus B Chem. Phys. Meteorol.* **1983**, *35*, 142–154. [[CrossRef](#)]
6. Vincent, E.M.; Madec, G.; Lengaigne, M.; Vialard, J.; Koch-Larrouy, A. Influence of tropical cyclones on sea surface temperature seasonal cycle and ocean heat transport. *Clim. Dyn.* **2012**, *41*, 2019–2038. [[CrossRef](#)]
7. Zheng, Z.-W.; Ho, C.-R.; Zheng, Q.; Lo, Y.-T.; Kuo, N.-J.; Gopalakrishnan, G. Effects of preexisting cyclonic eddies on upper ocean responses to Category 5 typhoons in the western North Pacific. *J. Geophys. Res. Ocean.* **2010**, *115*, C09013. [[CrossRef](#)]
8. Shay, L.K.; Goni, G.J.; Black, P.G. Effects of a Warm Oceanic Feature on Hurricane Opal. *Mon. Weather Rev.* **2000**, *128*, 1366–1383. [[CrossRef](#)]
9. Goni, G.J.; Trinanes, J.A. Ocean thermal structure monitoring could aid in the intensity forecast of tropical cyclones. *Eos* **2003**, *84*, 573–578. [[CrossRef](#)]
10. Lin, I.I.; Wu, C.C.; Emanuel, K.; Lee, I.H.; Wu, C.R.; Pun, I.F. The interaction of Super typhoon Maemi (2003) with a warm ocean eddy. *Mon. Weather Rev.* **2005**, *133*, 2635–2649. [[CrossRef](#)]
11. Scharroo, R.; Smith, W.H.F.; Lillibridge, J. Satellite altimetry and the intensification of Hurricane Katrina. *Eos* **2005**, *86*, 366. [[CrossRef](#)]
12. Chen, G.; Li, Y.; Xie, Q.; Wang, D. Origins of Eddy Kinetic Energy in the Bay of Bengal. *J. Geophys. Res. Ocean.* **2018**, *123*, 2097–2115. [[CrossRef](#)]

13. Cheng, X.; Xie, S.-P.; McCreary, J.P.; Qi, Y.; Du, Y. Intraseasonal variability of sea surface height in the Bay of Bengal. *J. Geophys. Res. Ocean.* **2013**, *118*, 816–830. [[CrossRef](#)]
14. Warner, J.C.; Armstrong, B.; He, R.; Zambon, J.B. Development of a Coupled Ocean–Atmosphere–Wave–Sediment Transport (COAWST) Modeling System. *Ocean Model.* **2010**, *35*, 230–244. [[CrossRef](#)]
15. Zambon, J.B.; He, R.; Warner, J.C. Investigation of hurricane Ivan using the coupled ocean–atmosphere–wave–sediment transport (COAWST) model. *Ocean Dyn.* **2014**, *64*, 1535–1554. [[CrossRef](#)]
16. Nelson, J.; He, R.; Warner, J.C.; Bane, J.M. Air–sea interactions during strong winter extratropical storms. *Ocean Dyn.* **2014**, *64*, 1233–1246. [[CrossRef](#)]
17. Renault, L.; Chiggiato, J.; Warner, J.C.; Gomez, M.; Vizoso, G.; Tintoré, J. Coupled atmosphere–ocean–wave simulations of a storm event over the Gulf of Lion and Balearic Sea. *J. Geophys. Res. Ocean.* **2012**, *117*. [[CrossRef](#)]
18. Prakash, K.R.; Pant, V.; Nigam, T. Effects of the Sea Surface Roughness and Sea Spray-Induced Flux Parameterization on the Simulations of a Tropical Cyclone. *J. Geophys. Res. Atmos.* **2019**, *124*, 14037–14058. [[CrossRef](#)]
19. Skamarock, W.C.; Klemp, J.B.; Dudhia, J.; Gill, D.O.; Barker, D.; Duda, M.G.; Huang, X.; Wang, W.; Powers, J.G. *A Description of the Advanced Research WRF Version 3 (No. NCAR/TN-475+STR)*; University Corporation for Atmospheric Research: Boulder, CO, USA, 2008. [[CrossRef](#)]
20. Nakanishi, M. Improvement of the Mellor–Yamada Turbulence Closure Model Based on Large-Eddy Simulation Data. *Bound.-Layer Meteorol.* **2001**, *99*, 349–378. [[CrossRef](#)]
21. Nakanishi, M.; Niino, H. An Improved Mellor–Yamada Level-3 Model with Condensation Physics: Its Design and Verification. *Bound. Layer Meteorol.* **2004**, *112*, 1–31. [[CrossRef](#)]
22. Nakanishi, M.; Niino, H. An Improved Mellor–Yamada Level-3 Model: Its Numerical Stability and Application to a Regional Prediction of Advection Fog. *Bound.-Layer Meteorol.* **2006**, *119*, 397–407. [[CrossRef](#)]
23. Nakanishi, M.; Niino, H. Development of an Improved Turbulence Closure Model for the Atmospheric Boundary Layer. *J. Meteorol. Soc. Jpn. Ser. II* **2009**, *87*, 895–912. [[CrossRef](#)]
24. NCEP. *NCEP FNL Operational Model Global Tropospheric Analyses, Continuing from July 1999*; NCEP: College Park, MD, USA, 2000. [[CrossRef](#)]
25. Chassignet, E.P.; Arango, H.; Dietrich, D.; Ezer, T.; Ghil, M.; Haidvogel, D.B.; Ma, C.-C.; Mehra, A.; Paiva, A.; Sirkes, Z. DAMÉE-NAB: The base experiments. *Dyn. Atmos. Ocean.* **2000**, *32*, 155–183. [[CrossRef](#)]
26. Haidvogel, D.B.; Arango, H.G.; Hedstrom, K.; Beckmann, A.; Malanotte-Rizzoli, P.; Shchepetkin, A.F. Model evaluation experiments in the North Atlantic Basin: Simulations in nonlinear terrain-following coordinates. *Dyn. Atmos. Ocean.* **2000**, *32*, 239–281. [[CrossRef](#)]
27. Umlauf, L.; Burchard, H. A generic length-scale equation for geophysical turbulence models. *J. Mar. Res.* **2003**, *61*, 235–265. [[CrossRef](#)]
28. Warner, J.C.; Sherwood, C.R.; Arango, H.G.; Signell, R. Performance of four turbulence closure models implemented using a generic length scale method. *Ocean Model.* **2005**, *8*, 81–113. [[CrossRef](#)]
29. Larson, J.; Jacob, R.; Ong, E. The Model Coupling Toolkit: A New Fortran90 Toolkit for Building Multiphysics Parallel Coupled Models. *Int. J. High Perform. Comput. Appl.* **2005**, *19*, 277–292. [[CrossRef](#)]
30. Jacob, R.L.; Larson, J.W.; Ong, E.T. M × N Communication and Parallel Interpolation in Community Climate System Model Version 3 Using the Model Coupling Toolkit. *Int. J. High Perform. Comput. Appl.* **2005**, *19*, 293–307. [[CrossRef](#)]
31. Prakash, K.R.; Pant, V. Upper oceanic response to tropical cyclone Phailin in the Bay of Bengal using a coupled atmosphere–ocean model. *Ocean Dyn.* **2016**, *67*, 51–64. [[CrossRef](#)]
32. Mohapatra, M.; Bandyopadhyay, B.K.; Tyagi, A. Best track parameters of tropical cyclones over the North Indian Ocean: A review. *Nat. Hazards* **2011**, *63*, 1285–1317. [[CrossRef](#)]
33. Prakash, K.R.; Nigam, T.; Pant, V. Estimation of oceanic subsurface mixing under a severe cyclonic storm using a coupled atmosphere–ocean–wave model. *Ocean Sci.* **2018**, *14*, 259–272. [[CrossRef](#)]
34. Nigam, T.; Prakash, K.R.; Pant, V. An assessment of the impact of oceanic initial conditions on the interaction of upper ocean with the tropical cyclones in the Arabian Sea. *J. Oper. Oceanogr.* **2019**, *13*, 121–137. [[CrossRef](#)]
35. Donlon, C.J.; Martin, M.; Stark, J.; Roberts-Jones, J.; Fiedler, E.; Wimmer, W. The Operational Sea Surface Temperature and Sea Ice Analysis (OSTIA) system. *Remote Sens. Environ.* **2011**, *116*, 140–158. [[CrossRef](#)]
36. Gröger, M.; Dieterich, C.; Meier, M.H.E.; Schimanke, S. Thermal air–sea coupling in hindcast simulations for the North Sea and Baltic Sea on the NW European shelf. *Tellus A Dyn. Meteorol. Oceanogr.* **2015**, *67*, 26911. [[CrossRef](#)]
37. Shetye, S.R.; Gouveia, A.D.; Shankar, D.; Shenoi, S.S.C.; Vinayachandran, P.N.; Sundar, D.; Michael, G.S.; Nampoothiri, G. Hydrography and circulation in the western Bay of Bengal during the northeast monsoon. *J. Geophys. Res. Ocean.* **1996**, *101*, 14011–14025. [[CrossRef](#)]
38. Vinayachandran, P.N.; Murty, V.S.N.; Babu, V.R. Observations of barrier layer formation in the Bay of Bengal during summer monsoon. *J. Geophys. Res. Ocean.* **2002**, *107*, SRF19. [[CrossRef](#)]
39. Rao, R.R. Seasonal variability of sea surface salinity and salt budget of the mixed layer of the north Indian Ocean. *J. Geophys. Res. Ocean.* **2003**, *108*, 9-1–9-14. [[CrossRef](#)]
40. Pant, V.; Girishkumar, M.S.; Bhaskar, T.V.S.U.; Ravichandran, M.; Papa, F.; Thangaprakash, V.P. Observed interannual variability of near-surface salinity in the Bay of Bengal. *J. Geophys. Res. Ocean.* **2015**, *120*, 3315–3329. [[CrossRef](#)]

41. ESR. 2009 OSCAR Third Deg. Ver. 1. PO.DAAC, CA, USA. Available online: https://podaac.jpl.nasa.gov/dataset/OSCAR_L4_OC_third-deg (accessed on 10 November 2019). [[CrossRef](#)]
42. Wada, A.; Usui, N. Importance of tropical cyclone heat potential for tropical cyclone intensity and intensification in the Western North Pacific. *J. Oceanogr.* **2007**, *63*, 427–447. [[CrossRef](#)]
43. Pun, I.-F.; Lin, I.-I.; Wu, C.-R.; Ko, D.-S.; Liu, W.T. Validation and Application of Altimetry-Derived upper Ocean Thermal Structure in the Western North Pacific Ocean for Typhoon-Intensity Forecast. *IEEE Trans. Geosci. Remote Sens.* **2007**, *45*, 1616–1630. [[CrossRef](#)]
44. Menemenlis, D.; Campin, J.M.; Heimbach, P.; Hill, C.; Lee, T.; Nguyen, A.; Schodlok, M.; Zhang, H. ECCO2: High resolution global ocean and sea ice data synthesis. *Mercat. Ocean Q. Newslett.* **2008**, *31*, 13–21.
45. Gray, W.M. Global View of the Origin of Tropical Disturbances and Storms. *Mon. Weather. Rev.* **1968**, *96*, 669–700. [[CrossRef](#)]
46. Singh, V.K.; Roxy, M.K.; Deshpande, M. Role of warm ocean conditions and the MJO in the genesis and intensification of extremely severe cyclone Fani. *Sci. Rep.* **2021**, *11*, 3607. [[CrossRef](#)] [[PubMed](#)]
47. Sil, S.; Gangopadhyay, A.; Gawarkiewicz, G.; Pramanik, S. Shifting seasonality of cyclones and western boundary current interactions in Bay of Bengal as observed during Amphan and Fani. *Sci. Rep.* **2021**, *11*, 22052. [[CrossRef](#)] [[PubMed](#)]
48. Pant, V.; Prakash, K.R. Response of Air–Sea Fluxes and Oceanic Features to the Coupling of Ocean–Atmosphere–Wave during the Passage of a Tropical Cyclone. *Pure Appl. Geophys.* **2020**, *177*, 3999–4023. [[CrossRef](#)]
49. Ren, D.; Lynch, M.; Leslie, L.M.; Lemarshall, J. Sensitivity of Tropical Cyclone Tracks and Intensity to Ocean Surface Temperature: Four Cases in Four Different Basins. *Tellus A: Dyn. Meteorol. Oceanogr.* **2014**, *66*, 24212. [[CrossRef](#)]